# Applications of Long-wavelength 256x256 Quantum Well Infrared Photodetector (QWIP) Hand-held Camera

**S. 1). Gunapala, '1'. N. Krabach, S. V. Bandara, J. K. Liu, and M. Sundaram**

Center for Space Microelectronics '1'ethnology. Jet f'repulsion Laboratory, California Institute of Technology, Pasadena, CA 91109

## ABSTRACT

A 9 μm cutoff 256x256 hand-held quantum well infrared photodetector (QWIP) camera has been demonstrated. Excellent imagery, with a noise equivalent differential temperature (NEΔT) of 26 mK has been achieved. In this paper, we discuss the performance of this portable long-wavelength infrared camera in quantum efficiency, NEΔT, minimum resolvable temperature difference (MRTD), uniformity, etc. and its applications in science, medicine and defense.

## INTRODUCTION

There are myriad applications that require long-wavelength, large, uniform, reproducible, low cost, steady, low power dissipation, and radiation hard infrared (IR) focal plane arrays (FPAs). For example, the absorption lines of many gas molecules, such as oxygen, ozone, water, carbon monoxide, carbon dioxide, nitrous oxide and etc. occur in the wavelength region from 3 to 18 μm. Thus, IR imaging systems that operate in the long-wavelength IR (LWIR) region (6 - 18 μm) are also required in many space applications such as monitoring the global atmospheric temperature profiles, relative humidity profiles, cloud characteristics, and the distribution of minor constituents in the atmosphere[1]. In addition, 6-18 μm FPAs would be very useful in detecting cold objects such as ballistic missiles in midcourse (when hot rocket engine is not burning most of the emission peaks are in the 8-15 μm IR region)[2]. The GaAs based Quantum Well Infrared Photodetector (QWIP)[3,7] focal plane array (FPA) cameras tuned to narrow spectral bands are excellent candidates for spaceborne and ground based applications. Fabricated entirely from large bandgap materials which are easy to grow and process, it is now possible to obtain large uniform FPAs of QWIPs tuned to detect light at wavelengths from 6 to 25 μm in the GaAs/AlxGa1-xAs material system[3,7].

Improving QWIP performance depends largely on minimizing the parasitic current that plag ues all light detectors, the dark current (the current that flows through a biased detector in the dark, i.e., with no photons impinging on it). As we have discussed elsewhere[7,8], at temperatures above 45 K, the dark current of the QWIP is entirely dominated by classic thermionic emission of ground state electrons directly out of the well into the energy continuum. Minimizing this last component" is critical to the commercial success of the QWIP as it allows the highly - desirable high-temperature camera operation.

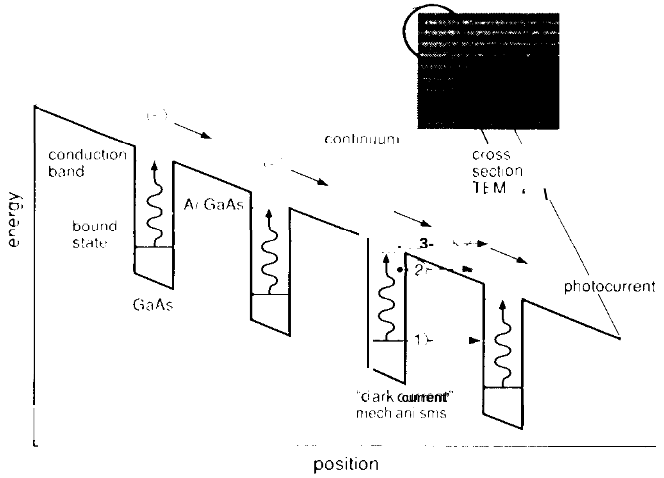


*Figure 1. Schematic diagram of the conduction band in a bound-to-quasibound QWIP in an externally applied electric field. Absorption of IR photons can photoexcite electrons from the ground state of the quantum well into the continuum, causing a photocurrent. Three dark current mechanisms are also shown: ground state tunneling (1); thermally assisted tunneling (2); and thermionic emission (3). The inset shows a cross-section transmission electron micrograph of a QWIP sample.*

Therefore, we have designed the bound-to-quasibound quantum well by placing the first excited state exactly at the well top as shown in Figure 1. The previous QWIPs were called the bound-to-continuum, because the first excited state was a continuum energy band above the well top (typically 10 meV). Dropping the first excited state to the well top causes the barrier to thermionic emission (roughly the energy height from the ground state to the well top) to be ~ 10 meV more in our bound-to-quasibound QWIP than in the bound-to-continuum one, causing the dark current to drop by a factor of ~ 6 at a temperature of 70 K[6,9].

# IMAGING FOCAL PLANE ARRAYS

Each period of the multi-quantum well (MQW) structure consists of a 45 Å well of GaAs (doped $n = 4\times10^{17}$ cm$^{-3}$) and a 500 Å barrier of $Al_{0.3}Ga_{0.7}As$. Stacking many identical quantum wells (typically 50) together increases photon absorption. Ground state electrons are provided in the detector by doping the GaAs well layers with Si. This photosensitive MQW structure is sandwiched between 0.5 μm GaAs top and bottom contact layers doped $n = 5\times10^{17}$ cm$^{-3}$, grown on a semi-insulating GaAs substrate by molecular beam epitaxy (MBE). Then a 0.7 μm thick GaAs cap layer on top of a 300 Å $Al_{0.3}Ga_{0.7}As$ stop-etch layer was grown *in situ* on top of the device structure to fabricate the light coupling optical cavity. The MBE grown QWIP structure was processed into 200 μm diameter mesa test structures (area = $3.14\times10^{-4}$ cm$^2$) using wet chei cal etching, and Au/Ge ohmic contacts were porated onto (IIC lop and bottom contact layers.

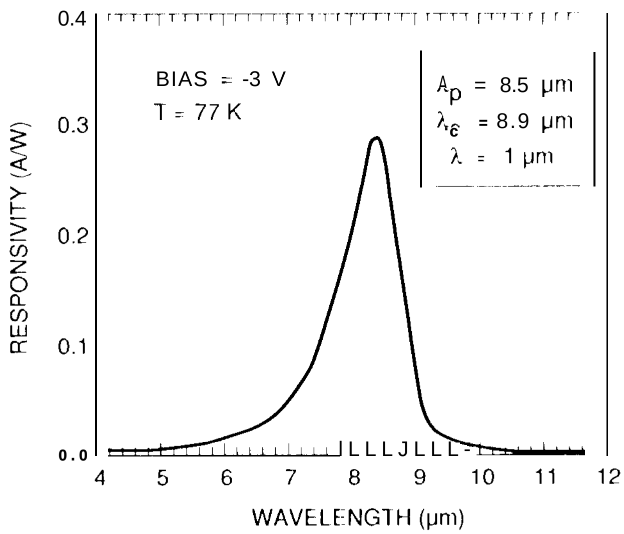


*Figure 2. Responsivity spectrum of a bound-to-quasibound LWIR QWIP test structure at temperature T = 77 K. The spectral response peak is at 8.5 μm and the long-wavelength cutoff is at 8.9 μm.*

The responsivity spectrum of the detectors in the FPA is shown in Figure 2. The responsivity of the detectors peak at 8.5 μm and the peak responsivity ($R_p$) is 300 mA/W at bias $V_B$ = -3 V. The spectral width and the cutoff wavelength are $\Delta\lambda/\lambda$ = 10% and $\lambda_C$ = 8.9 μm respectively. The peak quantum efficiency of the detectors was 6.9% at bias $V_B$ = -1 V. The lower quantum efficiency is due to the lower well doping density ($5\times10^{17}$ cm$^{-3}$) as it is necessary to suppress the dark current at the highest possible operating temperature. A peak quantum efficiency as high as 25% has already been achieved with regular well doping density (i.e., $1\times10^{18}$ cm$^{-3}$). Due to lower readout multiplexer well depth (i.e., $5\times10^{6}$ electrons) a lower dark current is mandatory to achieve a higher operating temperature. In this case, the highest operating temperature of 70 K was determined by the cooling capacity of the small Sterling cooler used in an Amber RADIANCE 1™ camera,

The photoconductive gain g was experimentally determined using[8] $g = i_n^2/4eI_DB + 1/2N$, where B is the measurement bandwidth, N is the number of quantum wells, and $i_n$ is the current noise, which was measured using a spectrum analyzer. The photoconductive gain of the detector reached 0.98 at $V_B$ = -5 V. Since the gain of QWIP is inversely proportional to lilt number of quantum wells N, the better comparison would be the well capture probability $p_c$, which is directly related to the gain[10] by $g = 1/Np_c$. The calculated well capture probabilities are 25% at low bias (i.e.. $V_B$ = -1 V) and 2% at high bias (i.e., $V_B$ = -5 V) which together indicate the excellent hot-electron transport in this (i~'vice structure. The peak detectivity is defined as $D_p^* = R_p\sqrt{AB}/i_n$, where $R_p$ is the peak responsivity, A is the area of the detector and A = $3.14\times10^{-4}$ cm$^2$. The measured peak detectivity at bias $V_B$ = -3.2 V and temperature T = 70 K is $2.3\times10^{11}$ cm$\sqrt{\text{Hz}}$/W. These detectors show background limited performance (BLIP) at bias $V_B$ = -2 V and temperature T = 72 K for 300 K background with f/2 optics.

It is well known that QWIPs do not absorb radiation incident normal to the surface unless the IR radiation have an electric field component normal to the layers of superlattice (growth direction)[8]. As we have discussed before[8,11] many more passes of IR light inside the detector structure can be obtained by incorporating a randomly roughened reflecting surface on top of the detectors which also removes the light coupling limitations and makes two dimensional QWIP imaging arrays feasible. This random structure was fabricated on the detectors by using standard photolithography and $CCl_2F_2$ selective dry etching. The advantage of the photolithographic process over a completely random process is the ability to accurately control the feature size and preserve the pixel to pixel uniformity which is a prerequisite for high sensitivity imaging FPAs.

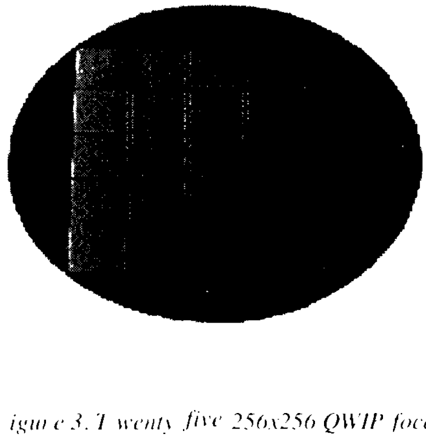

*Figure 3. Twenty five 256x256 QWIP focal plane arrays on a 3 in GaAs wafer*

After the random reflector array was defined by the lithography and dry etching, the photoconductive QWIPs of the 256x256 FPAs were fabricated by wet chemical etching through the photosensitive GaAs/$Al_xGa_{1-x}As$ multi-quantum well layers into the 0.5 µm thick doped GaAs bottom contact layer. The pitch of the FPA is 38 µm and the actual pixel size is 28x28 µm$^2$. The random reflectors on top of the detectors were then covered with Au/Ge and Au for Ohmic contact and reflection. Figure 3 shows twenty five processed QWIP FPAs on a 3 inch GaAs wafer. Indium bumps were then evaporated on top of the detectors for Si readout circuit (ROC) hybridization. A single QWIP FPA was chosen and hybridized (via indium bump-bonding process) to a 256x256 CMOS multiplexer (Amber AE-166) and biased at $V_B$ = -1.0 V. At temperatures below 72 K, the signal to noise ratio of the system is limited by array non-uniformity, multiplexer readout noise, and photo current (photon flux) noise. At temperatures above 72 K, temporal noise due to the QWIP's higher dark current becomes the limitation. As mentioned earlier this higher dark current is due to thermionic emission and thus causes the charge storage capacitors of the readout circuitry to saturate. Since the QWIP is a high impedance device, it should yield a very high charge injection coupling efficiency into the integration capacitor of the multiplexer. In fact Bethea *et al.*[3] have demonstrated charge injection efficiencies approaching 90%. Charge injection efficiency can be obtained from[4].

$$\eta_{inj} = \frac{g_m R_{Det}}{1+g_m R_{Det}}\left[\frac{1}{1+\dfrac{j\omega C_{Det} R_{Det}}{1+g_m R_{Det}}}\right] \qquad (1)$$

where $g_m$ is the transconductance of the MOSFET and it is given by $g_m = eI_{Det}/kT$. The differential resistance $R_{Det}$ of the pixels at -1 V bias is $4.5\times10^{10}$ Ohms at T=70 K and detector capacitance $C_{Det}$ is $3.0\times10^{-14}$ F. The detector dark current $I_{Det}$ = 14 pA under the same operating conditions. According to equation (1) the charge injection efficiency $\eta_{inj}$=90% at a frame rate of 30 Hz. The FPA was back-illuminated through the flat thinned substrate membrane (thickness ≈ 1300 Å). This initial array gave excellent images with 99.98% of the pixels working (number of dead pixels ≈ 10), demonstrating the high yield of GaAs technology. The operability was defined as the percentage of pixels having noise equivalent differential temperature less than 100 mK at 300 K background and in this case operability happens to be equal to the pixel yield.

We have used the following equation to calculate the noise equivalent temperature difference NEΔT of the FPA.

$$NE\Delta T = \frac{\sqrt{AB}}{D_B^*(dP_B/dT)\sin^2(\theta/2)} \qquad (2)$$

where $D_B^*$ is the blackbody detectivity, $dP_B/dT$ is the derivative of the integrated blackbody power with respect to temperature, and $\theta$ is the field of view angle [i.e., $\sin^2(\theta/2) = (4f^2+1)^{-1}$, where f is the f number of the optical system]. Figure 4 shows the measured NEΔT of the FPA at an operating temperature of T = 70 K, bias $V_B$ = -1 V for 300 K background and the mean value is 26 mK. This agrees reasonably with our estimated value of 8 mK based on test structure data. The peak quantum efficiency of the FPA was 3.3% (lower focal plane array quantum efficiency is attributed to 54% fill factor and 90% charge injection efficiency) and this corresponds to an average of three passes of IR radiation (equivalent to a single 45° pass) through the photosensitive multi-quantum well region.

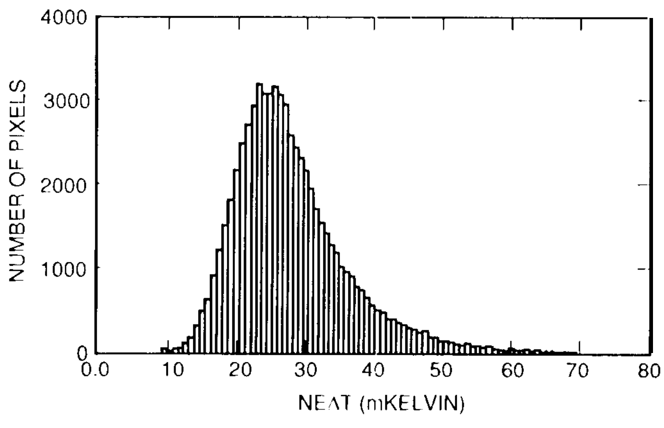


*Figure 4. Photosignal histogram of the 65,536 pixels of the 256x256 array showing a high uniformity of the FPA. The uncorrected non-uniformity (= standard deviation/mean) of the FPA is only 6.8% including 1% non-uniformity of ROC and 1.4% non-uniformity due to the cold-stop not being able to give the same field of view to all the pixels in the FPA.*

## HAND-HELD QWIP CAMERA

A 256x256 QWIP FPA hybrid was mounted onto a 250 mW integral Sterling closed-cycle cooler assembly and installed into an Amber RADIANCE 1™ camera-body, to demonstrate a hand-held LWIR camera (shown in Figure 5). The camera is equipped with a 32-bit floating-point digital signal processor combined with multi-tasking software, providing the speed and power to execute complex image-processing and analysis functions inside the camera body itself. The other element of the camera is a 100 mm focal length germanium lens, with a 5.5 degree field of view. It is designed to be transparent in the 8-12 μm wavelength range, to be compatible with the QWIP's 8.5 μm operation. The digital acquisition resolution of the camera is 12-bits, which determines the instantaneous dynamic range of the camera (i. e., 4096). However, the dynamic range of QWIP is 85 Decibels. Its nominal power consumption is less than 50 Watts.

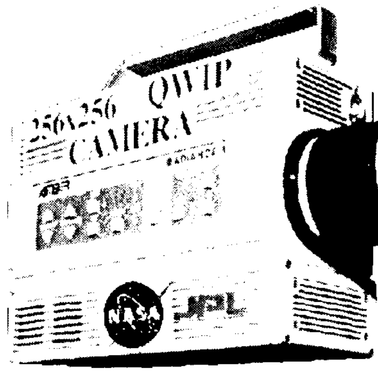


*Figure 5. Picture of the first 256x256 hand-held long wavelength QWIP camera (QWIP RADIANCE).*

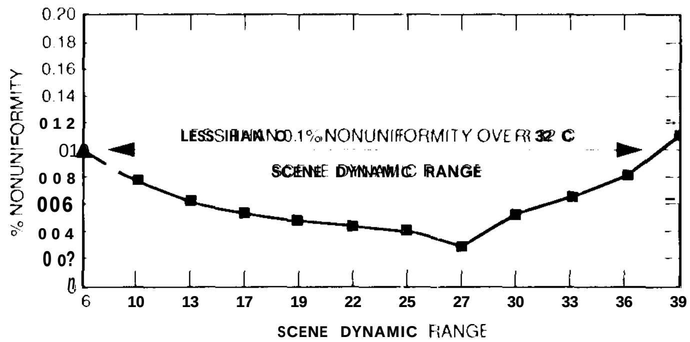


*Figure 6. Residual non-uniformity after two point correction as a function of scene temperature. This corrected non-uniformity range is comparable to 3 μm IR cameras.*

The measured mean NEΔT of the QWIP camera is 40 mK (the higher NEΔT is due to the 65% transmission through the lens assembly) at an operating temperature of T = 70 K and bias $V_B$ = -1.5 V, for a 300 K background. The uncorrected photocurrent non-uniformity (which includes a 1% non-uniformity of the ROC and a 1.4% non-uniformity due to the cold-stop in front of the FPA not yielding the same field of view to all the pixels) of the 65,536 pixels of the 256x256 FPA is about 6.8% (= sigma/mean). The non-uniformity after two-point (17° and 27° Celsius) correction improves to an impressive 0.05 %. As mentioned earlier, this high yield is due to the excellent GaAs growth uniformity and the mature GaAs processing technology. After correction, measurements of the residual non-uniformity were made at temperatures ranging from 10 Celsius (the cold temperature limit of the blackbody) up to 39 Celsius. The non-uniformity at each temperature was found by averaging 16 frames, calculating the standard deviation of the pixel-to-pixel variation of the 16 frame average and then dividing by the mean output, producing non-uniformity that may be reported as a percentage. For camera systems that have NEΔT of about 25 mK, the corrected image must have less than 0.1% non-uniformity in order to be TV quality. Only at a temperature of 39 Celsius did the camera's non-uniformity exceed the 0.1% non-uniformity threshold. Figure 6 shows non-uniformity plotted versus scene temperature. The 32 Celsius window where the correction is below 0.1% is based on the measured data and one extrapolated data point at 6 Celsius.

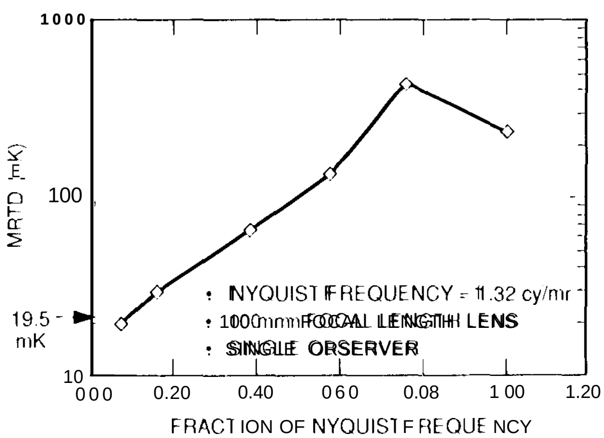


*Figure 7. Minimum resolvable temperature difference (MRTD) plotted as a function of the Nyquist frequency of 1.32 cy/mr. At 10% of the Nyquist frequency the MRTD was 19 mK*

The minimum resolvable temperature difference (MRTD) is shown in Figure 7. While the collection of the data does not adhere to the generally accepted requirements of having multiple observers, the data is consistent with the NEΔT measurement and worth reporting. Data was taken with seven bar targets ranging in spatial frequency from 0.1 cycles/milliradian up to 1.33 cy/mr, the first target where no contrast could be measured (unclear). At the lowest spatial frequency, the MRTD was 19 mK (or 19 mCelsius). Figure 7 shows MRTD plotted as a function of the Nyquist frequency of 1.32 cy/mr.

## APPLICATIONS

### FIREFIGHTING:

Video images were taken at a frame rate of 60 Hz at temperatures as high as T = 70 K, using a ROC capacitor having a charge capacity of 9x10⁶ electrons (the maximum number of photoelectrons and dark electrons that can be counted in the time taken to read each detector pixel). This infrared camera helped a Los Angeles TV news crew get a unique perspective on fires that raced through the Southern California seaside community of Malibu in October, 1996. The camera was used on the station's news helicopter. This portable camera features infrared detectors which cover longer wavelengths than previous portable cameras could. This allows the camera to see through smoke and pinpoint lingering hotspots which are not normally visible. This enabled the TV station to transmit live images of hotspots in areas which appeared innocuous to the naked eye. These hotspots were a source of concern and difficult for firefighters, because they could flare up even after the fire appeared to have subsided. Figure 8 shows the comparison of visible and infrared images of a just burned area as seen by the news crew in nighttime. It works effectively in both daylight and nighttime conditions. The event marked the QWIP camera's debut as a fire observing device.

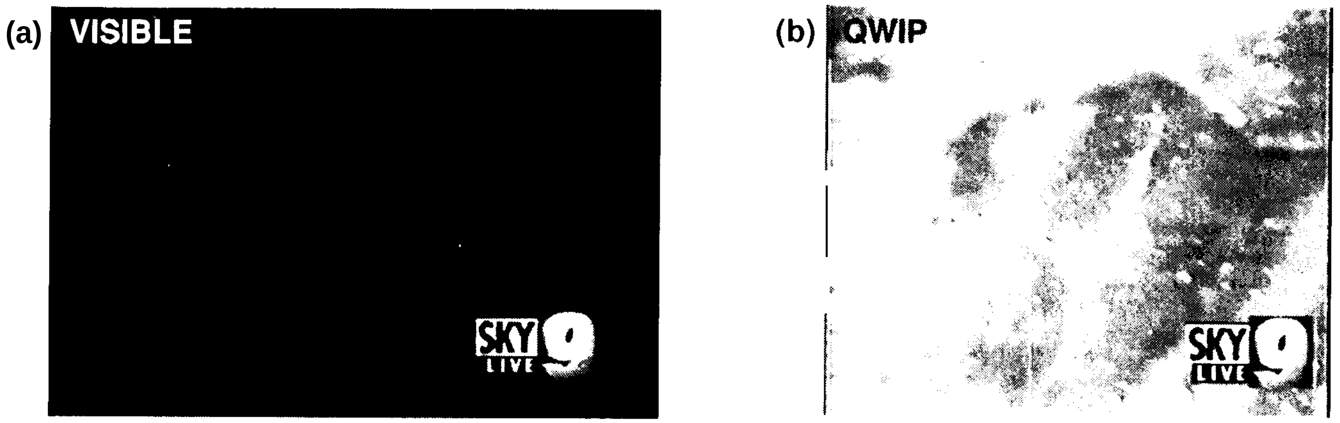


*Figure 8. Comparison of visible and infrared images of a just burned area as seen by a highly sensitive visible CCD camera and the long wavelength infrared camera in nighttime. (a) Visible image from a CCD camera. (b) Image from the 256x256 portable QWIP camera. This portable camera features infrared detectors covers longer wavelengths than previous portable cameras could. This allows the camera to see through smoke and pinpoint lingering hotspots which are not normally visible. This enables firefighters to locate the hotspots in areas which appeared innocuous to the naked eye. These hotspots are a source of concern and difficulty for firefighters, because fire can flare up even after it appears to have subsided. It works effectively in both daylight and nighttime conditions.*

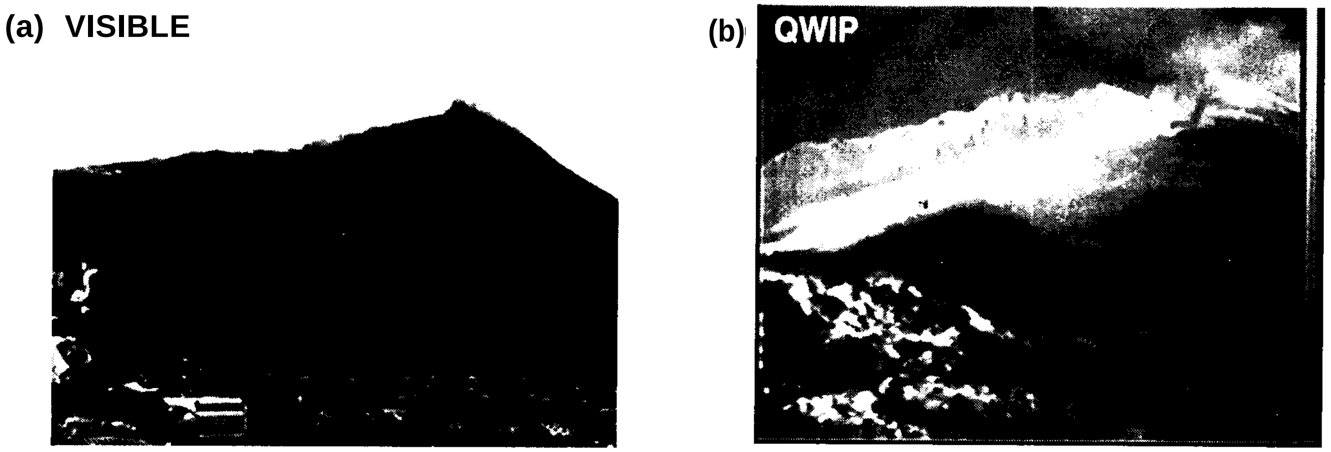


*Figure 9. Comparison of visible and infrared images of the Mount Kilauea Volcano in, Hawaii. (a) Visible image from a highly sensitive CCD camera. (b) Image from the 256x256 portable QWIP camera. The wide dynamic range enabled us to image volcanic features at temperatures much higher (300 - 1000 C) than can be imaged with conventional thermal imaging systems in the 3 - 5 μm range or in visible. The infrared image of the volcano clearly show a hot lava tube running underground which is not visible to the naked eye. This demonstrates the advantages of long wavelength infrared in geothermal mapping.*

## VOLCANOLOGY:

Recently, the camera has been used to observe volcanoes, mineral formations, weather and atmospheric conditions. This QWIP camera was taken to the Kilauea Volcano in, Hawaii. The objectives of this trip were to map geothermal features. The wide dynamic range enabled us to image volcanic features at temperatures much higher (300 - 1000 C) than can be imaged with conventional thermal imaging systems in the 3 - 5 μm range or in visible. Figure 9 shows the comparison of visible and infrared images of the Mount Kilauea Volcano in, Hawaii. The infrared image of the volcano clearly shows a hot lava tube running underground which is not visible to the naked eye.

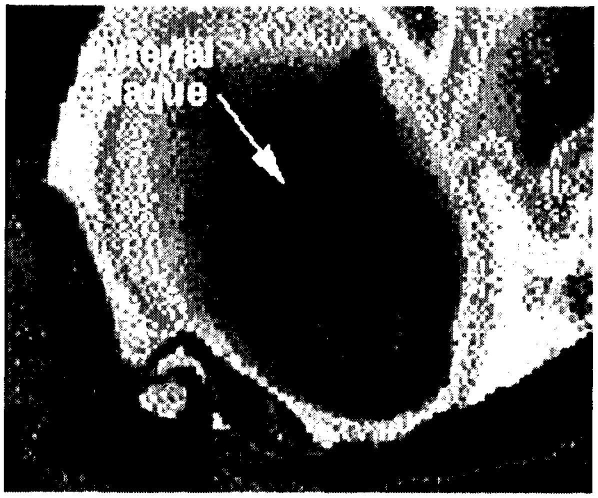

*Figure 10. This image shows arterial plaque deposited in a rabbit heart*

## MEDICINE:

This QWIP RADIANCE camera had limited exposure in the medical community as well. A group of researchers from the State University of New York in Buffalo and Walter Reed Army Institute of Research in Washington DC has used in the Dynamic Area Telethermometry (DAT). DAT has been used to study the physiology and patho-physiology of cutaneous perfusion, which has many clinical applications. DAT involves accumulation of hundreds of consecutive IR images and fast Fourier transform (FFT) analysis of the biomodulation of skin temperature, and of the microhomogeneity of skin temperature (HST, which measures the perfusion of the skin's capillaries). The FFT analysis yields the thermoregulatory frequencies and amplitudes of temperature and HST modulation. To obtain reliable DAT data, one needs an IR camera in the >8 μm range (to avoid artifacts of reflections of modulated emitters in the environment) a repetition rate of 30 Hz (allowing accumulation of a maximal number of images during the observation period (to maximize the resolution of the FFT), frame to frame instrumental stability (to avoid artifact stemming from instrument modulation) and sensitivity of less than 50 mK. According to these researchers the longer wavelength operation, higher spatial resolution, higher sensitivity and greater stability of the QWIP RADIANCE made it the best choice of all IR cameras.

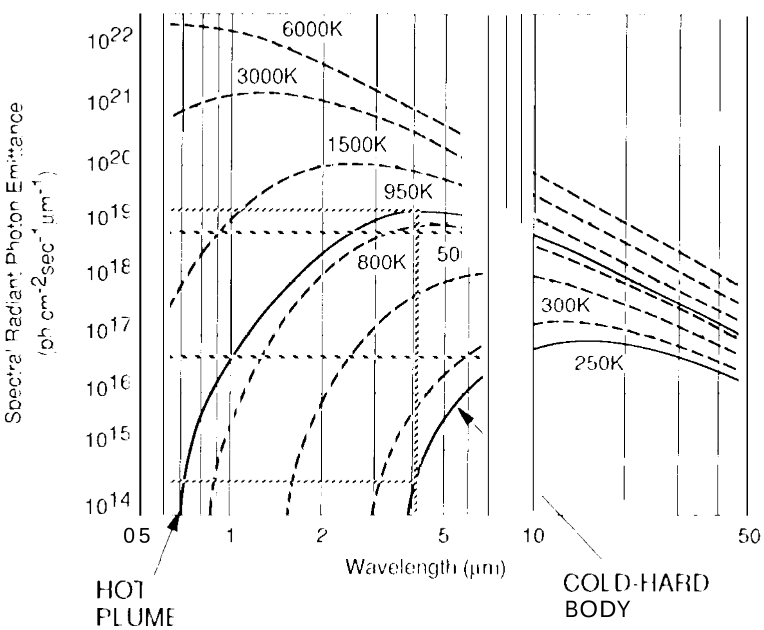


*Figure 11. Blackbody spectral radiant photon emittance at various temperatures*

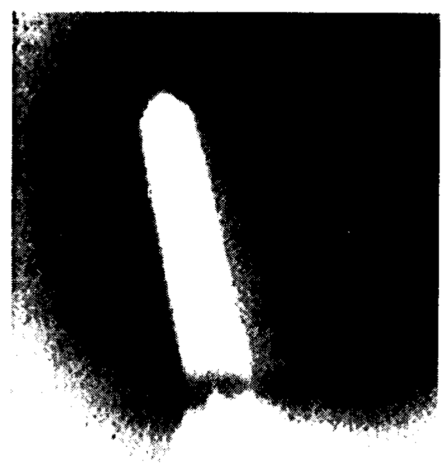

*Figure 12. Image of a Delta-II launch vehicle taken with the long-wavelength QWIP RADIANCE during the launch. This clearly indicates the advantage of long-wavelength QWIP cameras in the discrimination and identification of cold launch vehicles in the presence of hot plume during early stages of launch*